Available online at www.sciencedirect.com
ScienceDirect
Progress in Natural Science 18 (2008) 1077–1081
Progress in Natural Science
www.elsevier.com/locate/pnsc

Rapid spin–lattice relaxation time mapping incorporating flip angle calibration in quantitative magnetic resonance imaging

Zhongliang Zu [a], Qi Liu [a], Yanming Yu [a], Song Gao [b], Shanglian Bao [a,*]

[a] *The Key Laboratory of Medical Physics and Engineering, Peking University, Beijing 100871, China*
[b] *Medical Physics Department, Health Science Center of Peking University, Beijing 100083, China*

Received 21 January 2008; received in revised form 26 February 2008; accepted 26 February 2008

Abstract

Driven equilibrium single pulse observation of T_1 (DESPOT1) is a rapid spin–lattice relaxation constant (T_1) mapping technique in magnetic resonance imaging (MRI). However, DESPOT1 is very sensitive to flip angle (FA) inhomogeneity, resulting in T_1 inaccuracy. Here, a five-point DESPOT1 method is proposed to reduce the sensitivity to FA inhomogeneity through FA measurement and calibration. Phantom and *in vivo* experiments are performed to validate the technique. As a result, a rapid and accurate T_1 mapping is acquired by using the proposed five-point DESPOT1 method.

Keywords: Spin–lattice relaxation time; Flip angle inhomogeneity; Flip angle calibration

1. Introduction

Knowledge of spin–lattice relaxation time (T_1) can be used in different applications of magnetic resonance imaging (MRI), including discrimination among pathologic and normal tissue [1], contrast optimization [2], substructure studies of materials [3], and perfusion studies with either exogenous or endogenous contrast agents [4]. Many methods have been proposed to estimate T_1, such as inversion recovery (IR) [5], "two-point" method [6], Look–Locker method [7], and progressive saturation [8]. Unfortunately, these conventional sequences require long acquisition time. To accelerate data acquisition, several new approaches have been proposed recently.

Driven equilibrium single pulse observation of T_1 (DESPOT1) is a rapid T_1 mapping technique that is based on acquisition of a pair of spoiled gradient recalled echo (SPGR) images [9]. From the two SPGR images acquired with constant repetition time (TR) and varied flip angle (FA), T_1 can be extracted through a linearization of the SPGR signal equation. However, the accuracy of this method is quite sensitive to FA inhomogeneity, especially at high-field strength. FA inhomogeneity always arises from the wave behavior of radio frequency (RF) pulses, RF penetration, eddy current, or coil configuration effects due to imperfect hardware or electromagnetic properties of the object imaged [10]. Therefore, it is necessary to compensate for the imperfections in FA distribution when DESPOT1 is used on high-field MRI scanner.

Wang et al. have calibrated FA inhomogeneity in T_1 measurement based on measurement of the FA distribution using two EPI images [11]. However, image distortion inevitably occurs in EPI imaging resulting in errors in FA measurement. In this work, we present a five-point DESPOT1 method to map T_1 accurately and rapidly. The method performs three SPGR imagings at three large FAs α_1, α_2, and α_3 near 180° in order to get FA distribution and two SPGR imagings at two optimized FAs α_4 and α_5 for T_1 mapping. With the knowledge of FA distribution,

* Corresponding author. Tel./fax: +86 10 62751880.
E-mail address: bao@pku.edu.cn (S. Bao).

1002-0071/$ - see front matter © 2008 National Natural Science Foundation of China and Chinese Academy of Sciences. Published by Elsevier Limited and Science in China Press. All rights reserved.
doi:10.1016/j.pnsc.2008.02.010

the inaccuracy of T_1 mapping can be calibrated and corrected. Phantom and *in vivo* experiments demonstrate that our proposed five-point DESPOT1 method is a rapid and accurate T_1 mapping technique.

2. Materials and methods

2.1. Measurement of FA scaling factor

FA scaling factor $r(x,y)$ is a ratio between the actual FA α_a and nominal FA α_n at position (x,y), which can be calculated from three SPGR images using a recently proposed method called 180° signal null [12]. The general SPGR signal equation with FA α can be written as [12]

$$M = \frac{M_0(1-E_1)\sin(\alpha)}{1-E_1\cos(\alpha)}, \tag{1}$$

where M_0 is the magnetization at thermal equilibrium and $E_1 = \exp(-TR/T_1)$.

Fig. 1 is a plot of M versus α according to Eq. (1). When $\alpha_\alpha = 180°$, the signal intensity is zero. Thus, the nominal FA at $M = 0$, which is named α_n^{null}, corresponds to $\alpha_\alpha = 180°$. Therefore, the FA scaling factor $r(x,y)$ can be determined [12] as

$$r(x,y) = \frac{180^\circ}{\alpha_n^{\text{null}}(x,y)}. \tag{2}$$

From Fig. 1 it is easy to find that M varies approximately linearly with respect to FA near 180°. By performing several SPGR imagings with different FAs near 180°, the corresponding signal intensities may be fitted to a straight line to determine $\alpha_n^{\text{null}}(x,y)$, which is the cross point between the fitted line and the abscissa. According to Eq. (2), $r(x,y)$ can also be calculated. In this work, in the aim of shorter total imaging time, we propose performing three SPGR imagings at FAs $\alpha_1 = 180° - \beta$, $\alpha_2 = 180°$, and $\alpha_3 = 180° + \beta$, where β needs to be optimized according to prior knowledge of the range of r.

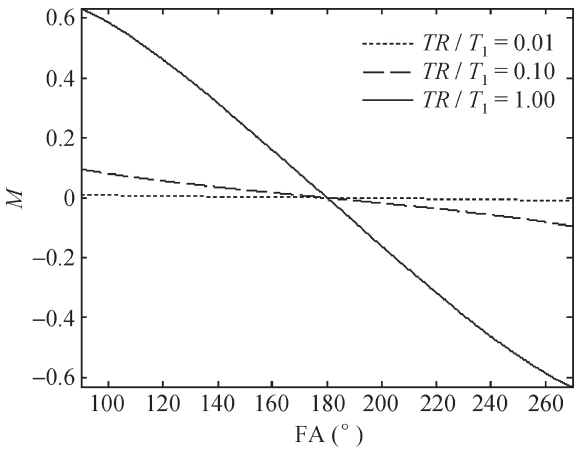

Fig. 1. Plot of SPGR signal versus FA near 180° for a range of TR/T_1.

2.2. Measurement of T_1 with FA correction terms

Eq. (1) can be represented in the linear form, $Y = kX + l$ as [9]

$$\frac{M}{\sin(\alpha)} = E_1\frac{M}{\tan(\alpha)} + M_0(1-E_1). \tag{3}$$

With two SPGR data sets at FA α_4 and α_5, the slope k can be estimated from Eq. (3), allowing T_1 to be extracted:

$$T_1 = -TR/\ln(k). \tag{4}$$

2.3. FA optimization

On 3 T scanner, the FA scaling factor is usually within the range $0.75 \leqslant r \leqslant 1.25$ for water phantom, which means that $135° \leqslant \alpha_a \leqslant 225°$ when $\alpha_n = 180°$. Within this range, we believe it is a reasonable approximation to assume that the data can be fitted to a straight line, as seen in Fig. 1. Fig. 2(a) is a plot of error introduced by using linear regression with the three FAs versus β. The error is expressed as an average of the relative deviation of the fitted value $\alpha_n^{\text{null}}(x,y)$ from 180° over the range of r. The highest degree

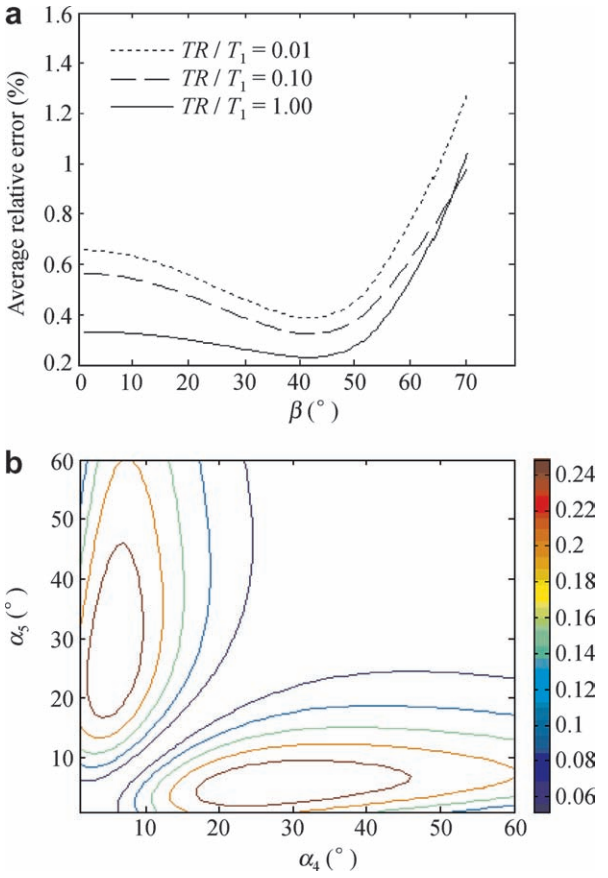

Fig. 2. (a) Plot of the average relative error introduced by linear fitting versus β for $TR/T_1 = 0.01$, 0.10, 1.00, respectively. (b) The dynamic range DR as a function of the prescribed α_4 and α_5 at $TR = 33$ ms and $T_1 = 50$ ms, which is similar to the T_1 value of the phantom used here. The optimum FAs are 25° and 5°.

of accuracy is achieved when $\beta = 42°$. Therefore, the optimum FAs for the three SPGR imagings are 138°, 180°, and 222°, respectively.

The two FAs α_4 and α_5 used in T_1 mapping can be optimized according to the linear form of SPGR signal equation in (3). We define a dynamic range (DR) of regression line as [9]

$$\mathrm{DR} = \left(\frac{M\alpha_5}{M_0 \sin(\alpha_5)} - \frac{M\alpha_4}{M_0 \sin(\alpha_4)}\right) \times (M\alpha_5 + M\alpha_4). \quad (5)$$

Using Eq. (1), numerical calculation of the DR at all possible combinations of α_4 and α_5 can be achieved. Fig. 2(b) shows the simulation result at TR of 33 ms and T_1 of 150 ms, which is similar to the T_1 value of the phantom used here. Evaluation of the DR yields optimum FAs of 25° and 5° for DESPOT1.

2.4. Experiment

SPGR sequences with five optimized FAs were implemented on a General Electric 3 T Signa Excite scanner (General Electric, Milwaukee, WI). A spherical phantom filled with distilled water and $NiSO_4$ was used to verify the proposed method. Acquisition parameters were $TR/TE = 33/6$ ms, 256×256 matrix, 30×30 cm field of view (FOV) and 5 mm slice thickness. The FA distribution was calculated from the three image sets with $\alpha_1 = 138°$, $\alpha_2 = 180°$, and $\alpha_3 = 222°$. T_1 map was calculated from the two image sets with $\alpha_4 = 25°$ and $\alpha_5 = 5°$ according to Eqs. (3) and (4), in which FA calibration was considered.

Raw data were first collected from the scanner, and then complex images were acquired by performing image reconstruction offline. Linear regression analysis of intensity versus α_n for each pixel was implemented in Matlab 6.5 (The Math Works, Natick, Ma) to determine $\alpha_n^{\mathrm{null}}(x,y)$, and hence $r(x,y)$ by using Eq. (2). The sign of the magnitude signal intensity was determined from the complex images by monitoring the change in sign of the complex data set. FA distribution was then acquired by multiplying r by α_n. Assuming that the FA distribution varies smoothly, a low-pass filter was applied to the FA map in order to eliminate the influence of image noise on T_1 evaluation.

To ascertain *in vivo* applicability of this technique, the five-point DESPOT1 was performed on a healthy volunteer. Human tissue has low dielectric constant, which results in a lower variation in r than that would be observed with water phantom. Therefore, the FA scaling factor must be within the range $0.75 \leqslant r \leqslant 1.25$, and the optimum FAs α_1, α_2, and α_3 for water phantom can also be used here. For the optimization of α_4 and α_5, a T_1 of 1000 ms, which is similar to that of human brain tissue, was assumed. As a result, $\alpha_4 = 3°$ and $\alpha_5 = 12°$ were found to be the optimum FAs through simulation. Other imaging parameters were similar to that used in phantom experiment.

An IR-SE sequence was also performed to get T_1 map of phantom containing eight tubes with various concentrations of $MnCl_2$, providing several T_1 values ($T_1 \approx 250$, 350, 500, 700, 1200, 1500, 2000, 2500 ms). The T_1 value (an average value from a region of interest within each tube) was used as a reference.

3. Results

3.1. Phantom study

Fig. 3(a) and (b) show phantom T_1 map with traditional DESPOT1 and the five-point DESPOT1 method, respectively. Fig. 3(c) shows the profiles extracted through the phantom T_1 map along the right/left direction as indicated by the lines in Fig. 3(a) and (b). The dotted line shows an increase of the signal intensity toward the center of the phantom T_1 map, while the solid line is smoother, which indicates that our proposed method is less sensitive to FA inhomogeneity.

3.2. In vivo study

Fig. 4 shows the brain T_1 map from one healthy male subject (24-years-old). The arrow in Fig. 4(a), in which FA inhomogeneity is not calibrated, indicates that the area receives a higher RF field than the periphery, resulting in misevaluation of T_1 map. While in Fig. 4(b), where the five-point DESPOT1 method is used, the T_1 values in the same region are correctly evaluated. The resulting values for gray matter (GM), white matter (WM), and cerebrospinal fluid (CSF) are about 1390 ± 12 ms, 852 ± 7 ms, and

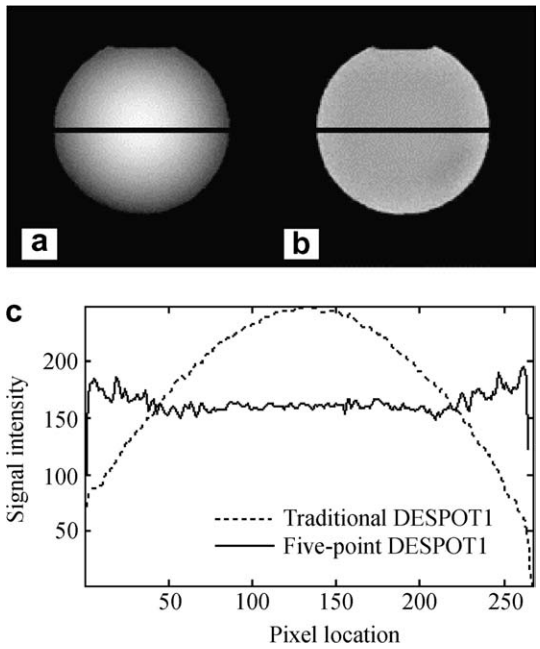

Fig. 3. Phantom T_1 map with (a) traditional DESPOT1 method and (b) five-point DESPOT1 method. Profiles in (c) are extracted through the phantom T_1 map in (a) and (b) along the right/left direction as indicated by the lines.

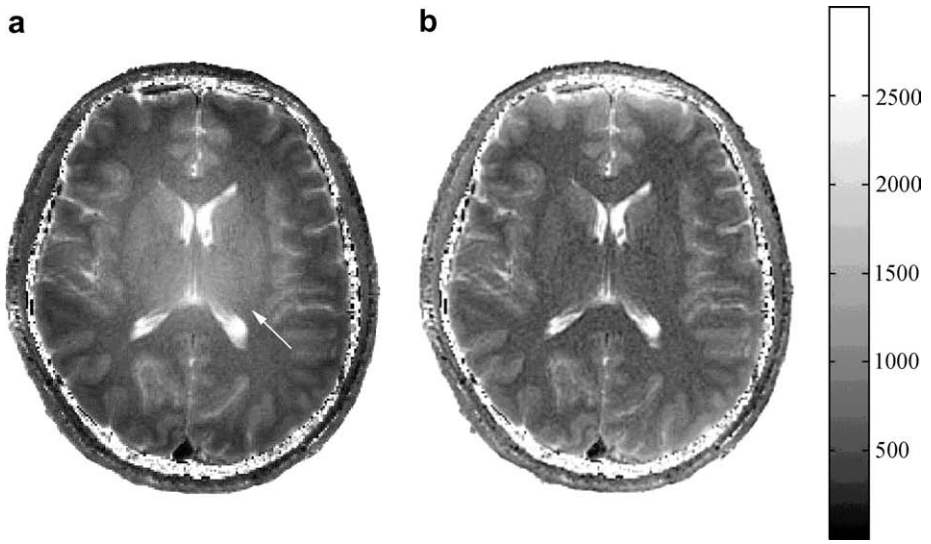

Fig. 4. Human brain T_1 map using (a) traditional DESPOT1 method and (b) five-point DESPOT1 method.

2217 ± 28 ms, respectively, which are similar to the literature values published in other articles [11].

4. Discussion

Traditional T_1 mapping methods require a long acquisition time, which limits their uses in many clinical applications. DESPOT1 permits rapid determination of T_1 on 1.5 T scanner, where FA distribution is homogenous. However, on a high-field scanner, such as 3 T or 7 T, DESPOT1 cannot provide accurate result. To solve this problem, we propose a five-point DESPOT1 method, in which three SPGR images are acquired to calculate FA distribution and two SPGR images are used to calculate T_1 map. The total acquisition time of the proposed technique is only 2.5 times that of the traditional DESPOT1.

As the gold standard for T_1 mapping, IR-SE can provide accurate T_1 determination, which is not sensitive to FA inhomogeneity. We measured a phantom containing eight tubes using IR-SE and the proposed five-point DESPOT1 method. Linear regression analysis in Fig. 5 reveals a high correlation ($R^2 = 0.99$) between the two methods, confirming that no statistical difference exists between the groups.

The FA mapping method used here has some errors introduced by linear fitting although optimum angles were chosen. Fig. 6 shows the relative error versus FA scaling factor. The relative error increases when FA scaling factor deviates largely from 1.00. On ultrahigh-field scanner, where the signal intensity will no longer vary linearly with FAs, a non-linear fitting method and more SPGR images should be used to accurately determine FA distribution. In this work, the relative error introduced by linear fitting is 1.9% at most, which is acceptable compared with other sources of inaccuracy, such as non-ideal slice profile and partial volume averaging [14].

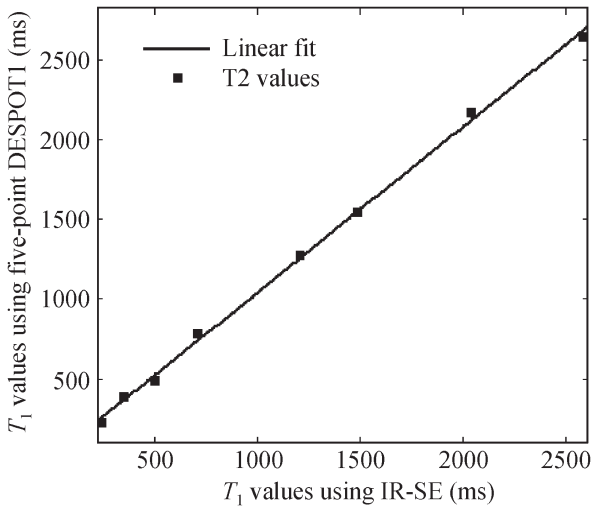

Fig. 5. Comparison of T_1 values (ms) of eight phantom tubes calculated from IR-SE data and five-point DESPOT1 data. The linear regression (solid line) indicates a good correlation between the two methods ($y = 1.04x + 2.3$, $R^2 = 0.99$).

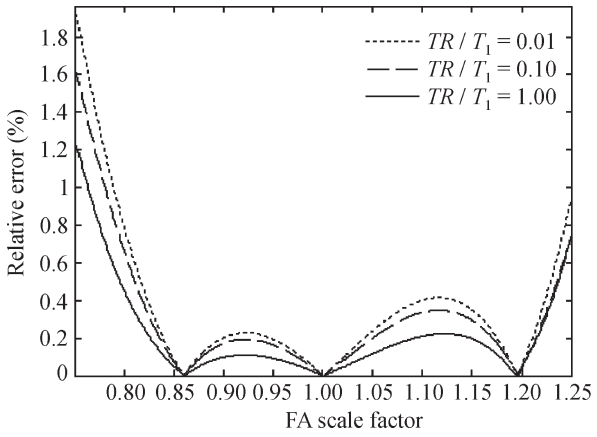

Fig. 6. Plot of relative error versus FA scaling factor r.

The FA scaling factors are determined using high FAs that are not conventionally used. It has been found that FA scaling factor varies slightly with nominal FA [11], which means that the achieved FA scaling factor at high FA might be different from that at low FA. However, with careful recalibration of RF transmitter, the FA scaling factor is verified to be valid for all FAs [13].

Measurement of multiple-component T_1 relaxation times is always required for the detection of macromolecules, such as in the diagnosis of multiple sclerosis. Although our proposed method can only provide mono-component T_1 measurement, it is enough for many important applications including imaging protocols optimization, perfusion imaging and contrast agent quantification.

5. Conclusions

In this work, we provide a five-point DESPOT1 method for rapid and accurate T_1 mapping. Phantom and *in vivo* experiments demonstrate that the sensitivity of the proposed five-point DESPOT1 to FA inhomogeneity is greatly reduced compared with traditional DESPOT1. Investigation of this method in terms of clinical applications is currently under way.

Acknowledgments

This work was supported by National Natural Science Foundation of China (Grant Nos. 10527003 and 60672104), the State Key Development Program for Basic Research of China (2006CB705700-05).

References

[1] Bottomley PA, Hardy CJ, Argersinger RE, et al. A review of ^{1}H NMR relaxation in pathology: are T_1 and T_2 diagnostic? Med Phys 1987;14:1–37.
[2] Vadim YuK, Alley MC. Differentiation between the effects of T_1 and T_2^* shortening in contrast-enhanced MRI of the breast. J Magn Reson Imaging 1999;9:172–6.
[3] Attard J, Hall L, Herrod N, et al. Materials mapped with NMR. Phys World 1991;4:41–5.
[4] Jackson EF, Narayana PA, Wolinsky JS, et al. Accuracy and reproducibility in volumetric analysis of multiple sclerosis lesions. J Comput Assist Tomogr 1993;17:200–5.
[5] Hahn EL. An accurate nuclear magnetic resonance method for measuring spin–lattice relaxation times. Phys Rev 1949;76:145–6.
[6] Freeman R, Hill HDW, Kaptein R. An adaptive scheme for measuring NMR spin–lattice relaxation times. J Magn Reson 1972;7:82–98.
[7] Look DC, Locker DR. Time saving in measurement of NMR and EPR relaxation times. Rev Sci Instrum 1970;41:250–1.
[8] Freeman R, Hill HDW. Fourier transform study of NMR spin–lattice relaxation by progressive saturation. J Chem Phys 1971;54:3367–77.
[9] Deoni SCL, Rutt BK, Peters TM. Rapid combined T_1 and T_2 mapping using gradient recalled acquisition in the steady-state. Magn Reson Med 2003;49:515–26.
[10] McVeigh ER, Bronskill MJ, Henkelman RM. Phase and sensitivity of receiver coils in magnetic resonance imaging. Med Phys 1986;13:806–14.
[11] Wang JH, Qiu ML, Kim H, et al. T_1 measurements incorporating flip angle calibration and correction in vivo. J Magn Reson 2006;182:283–92.
[12] Haacke EM, Brown RW, Thompson MR, et al. Magnetic resonance imaging: physical principles and sequence design. 1st ed. New York: John Wiley and Sons Press; 1999, [p. 454–55].
[13] Dowell NG, Tofts PS. Fast, accurate, and precise mapping of the RF field in vivo using the 180° signal null. Magn Reson Med 2007;58:622–30.
[14] Haacke EM, Brown RW, Thompson MR, et al. Magnetic resonance imaging: physical principles and sequence design. 1st ed. New York: John Wiley and Sons Press; 1999, [p. 657–661].